RESEARCH ARTICLE OPEN ACCESS

# Influence of plastic deformation gradients at room temperature on precipitation kinetics and mechanical properties of high-strength aluminum alloys

E. Scharifi*, A. Danilenko*, U. Weidig*, K. Steinhoff*
**(Metal Forming Technology, University of Kassel, Kurt-Wolters-Str. 3, 34125 Kassel, Germany)*
*(Corresponding Author: Emad Scharifi*

**ABSTRACT**
This work focuses on the influence of cold deformation gradients on precipitation kinetics and the resulting mechanical properties of two different high-strength aluminum sheet materials, AA6082 and AA7075. For this purpose, the investigated materials were solution heat treated and formed to different strain levels ranging from 0-18% in the supersaturated state after quenching in water. The respective strengthening behavior was reflected by uniaxial tensile tests and Vickers hardness measurement. Optical strain measurement based on the digital image correlation method was further used to determine and characterize the material-dependent local plastic deformation. It was found that pre-deformations at room temperature influence the strengthening process by accelerating the precipitation kinetic that is more obvious in case of AA7075. It is further indicated that the peak hardness depends strongly on the amount of deformation prior to ageing. This finding is linked to the increase of dislocation density generated during cold deformation. Experimental results based on digital image correlation measurements under tensile stress demonstrate a high formability and lower material strength for both materials in supersaturated condition. Localized strain in form of bands which propagate along the specimen gauge length was further observed using this technique. After aging treatment, no propagating shear-bands were observed. Local strain maps of post-tensioned specimens show a high plastic deformation concentration mainly in the regions with higher cold deformation degree.
**Keywords –** Heat treatment, High-strength aluminum alloys, Precipitation hardening, W-temper forming

---

Date Of Submission: 05-06-2019 Date Of Acceptance: 20-06-2019

---

## I. INTRODUCTION

Lightweight design is one of the main subjects in the transportation sector since the last decades. Legal regulations and global trends toward intense $CO_2$ reduction necessitate increasing efforts and more creative solutions than in the past [1]. Thus, aluminum alloys are widely used as lightweight engineering materials in the automotive and aerospace industry, due to their excellent strength-to-density ratio that allows the overall weight reduction of structures. For these application fields, the chosen alloys require to perform in a multitude of forming processes [2–4].

However, despite the favorable mechanical and physical properties, the formability of aluminum alloys in T6 condition at room temperature is due to the high material strength degree, very poor [5]. Other investigations carried out on the bending behavior of high-strength aluminum alloys show high springback as well as low formability at room temperature for complex-shaped components [6–8]. As an alternative, W-temper forming offers an approach to increase the formability and reduce springback in the resulting geometry. The so-called W-temper forming refers to room temperature deformation of sheet material after solutionizing and quenching in the supersaturated solid solution (SSSS) condition. Precipitation-hardenable aluminum alloys in this state exhibit lower material strength and hence improved ductility.

Argandoña et al. [9] for example investigated the W-temper formability of precipitation-hardenable AA7075 sheet material compared to hot stamping and room temperature forming process in the as-received T6-condition. For this purpose, a complex-shaped geometry, an automotive B-Pillar, was chosen to obtain complex stress-strain-path during deformation operation comparable to industrial conditions. The experimental results using W-temper and hot forming strategies revealed higher formability and dimensional accuracy compared to the T6 cold forming [6–8]. However, a slight appearance of springback after the forming step should be also taken into account in case of W-temper forming, although this phenomenon is less pronounced due to the reduced strength in the SSSS condition. Also, the interaction between the induced strain hardening during the forming operation and precipitation hardening process in a subsequent aging step has to

be adequately considered [10]. Cold deformation in the W-temper condition has a considerable impact on the material strengthening that can be adjusted after aging treatment. Investigation carried on the influence of pre-deformation have shown an improved efficiency of strengthening mechanisms during the aging step, leading to an increase in yield and ultimate tensile strength [11,12]. A remarkable decrease in artificial aging time and a significant change of the precipitation sequence caused by the pre-straining of the material was observed by Gazizov et al. [13]. This behavior and an increase in hardness of AA6023 alloy after the artificial aging was also observed by Martin et al. [14].

Despite the well known fact that the precipitation nucleation and growth during the aging step of aluminum heat treatments is affected by the degree of plastic deformation, until now only few research work exist on the influences of different strain levels on aging strategies on AA6082 and AA7075 during the W-temper forming. On top of that, there is a lack of knowledge about the particular influence of a graded logarithmic strain distribution of those alloys. Therefore, the present work aims at presenting the local deformation behavior of graded structures using DIC technique and the synergy of different pre-deformation levels and precipitation hardening for W-temper forming.

## II. MATERIAL DESCRIPTION AND EXPERIMENTAL INVESTIGATION

### 2.1. Materials

The experimental investigations in this work were carried out on heat treatable aluminum alloys AA6082, which is used commonly in automotive applications and AA7075, typically favored in aerospace structures. As-received, the material condition is given for both alloys to be T6 (solution heat treated, quenched and artificially aged). In this condition they exhibit a hardness of 115 HV and an ultimate tensile strength (UTS) of 345 MPa for AA6082 and 189 HV and 577 MPa for AA7075, respectively.

### 2.2. Experimental concept and program

The experimental set-up in the present study consists of a roller hearth furnace to heat and solutionize the material at the corresponding solution heat treatment (SHT) temperature. Cooling is performed in a water-aquatensid-mixture (W+AQ) that allows a high cooling rate while lower thermal distortion compared to water-quench is gained. For the artificial ageing of the investigated heat treatable aluminum alloys an air circulating furnace was used.
The first work package (WP) focuses on the effect of the impact of different cold deformation levels on the formability in W-temper condition, Figure 1 (a). Therefore, the investigated materials were firstly heated up to the recommended SHT temperatures 540 °C (AA6082) 480 °C (AA7075), respectively, and solutionized for 20 min [15]. In order to identify a deformation threshold level, samples were quenched in a water-aquatensid-mixture (W+AQ) after solutionizing and strained immediately at room temperature to an overall strain of 0, 3, 6, 12 and 18 %. Simultaneously, the local deformation behavior of the tensile samples was recorded using DIC technique. Afterwards, Vickers hardness measurements were carried out to reveal the strengthening behavior.

The second WP focuses on the influence of cold deformation on the mechanical properties concerning the precipitation kinetics during artificial aging. Therefore, the strained samples in W-temper condition (global strain of 0, 3, 6, 12 and 18 %) were aged in case of AA6082 for 8 hours at 165 °C and for 20 hours at 120 °C for AA7075, Figure 1 (b).

The third and last WP in this study deals with the local deformation behavior and the logarithmic strain distribution of the pre-strained samples after the artificial aging. Therefore, selected pre-deformed samples (global strain of 0, 6 and 18 %) with different deformation gradients were strained after artificial aging up to failure and the deformation behavior was simultaneously recorded using DIC technique.

### 2.3. Characterization of properties and local deformation behavior

Hardness profiles along the longitudinal axes of each tensile sample were obtained from Vickers hardness measurements. Cold deformation were conducted using uniaxial tensile tests on a Hegewald & Peschke screw driven testing machine (force capacity: 100 kN) with an extensometer attached at the gauge length. The tensile samples were machined by electrical discharge machining in two different geometries, a new and a standard geometry,

Figure 2. The new geometry, which was used for WP 1 and 2, is chosen, in order to influence the stress distribution during the tensile test and thus to concentrate the plastic deformation mainly to the section with the smallest gauge width but also to create strain gradients along the complete gauge length. Afterwards a standard sample with a homogeneous cross-section is taken from the new designed one for the experiments of WP 3,

Figure 2 (b).

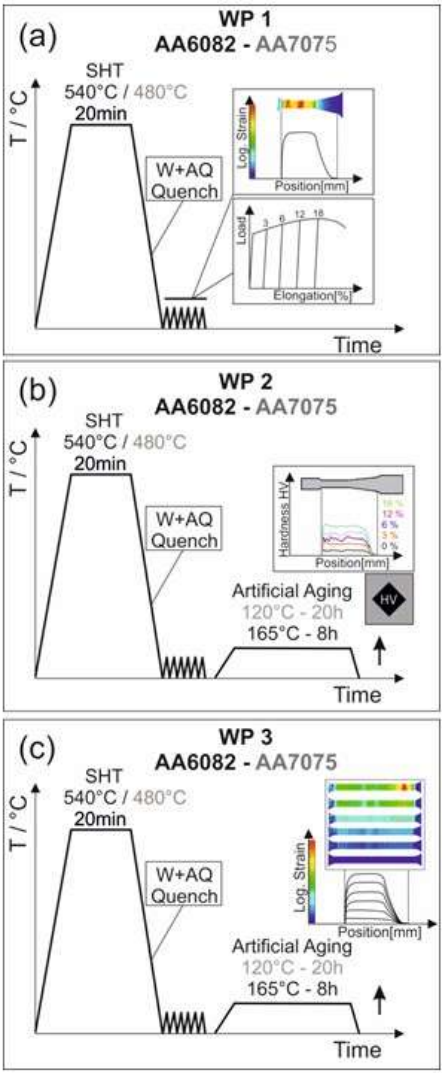


**Figure 1:** Schematic illustration of the investigated forming processes routes and working packages.

In order to measure the local strain of the investigated material, DIC measurements coupled with the tensile testing machine were carried out. For this aim, a high contrast surface pattern was applied by two different colors sprayed on the tensile specimen surface. The local strain measurement was conducted using two CCD cameras focused on the tensile specimen surface. The described measurement was performed by the ARAMIS software (GOM - Gesellschaft für Optische Messtechnik mbH, Germany).

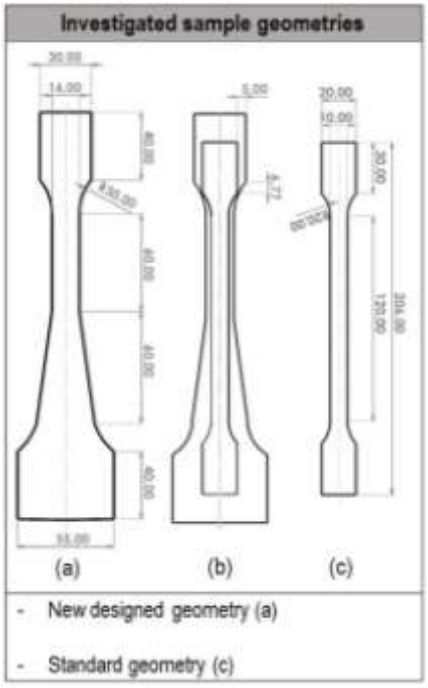


**Figure 2:** Used sample geometries with different gauge widths. (a) The new design sample geometry to obtain different deformation gradients along the entire gauge length. (b) Location of standard tensile sample taken from the new design geometry sample after pre-deformation. (c) Standard tensile geometry.

## III. RESULTS

### 3.1. Macroscopic deformation behavior in W-temper state and effect of different deformation levels on strengthening

Figure 3 (a) shows the local deformation behavior of AA6082 during tensile test in W-temper condition immediately after solutionizing at 540 °C for 20 min and quenching in W+AQ-mixture. As it can be seen from this figure, the plastic deformation appears mainly within the smallest gauge width from 10-70 mm on the tensile specimen. This behavior is induced by the particular new designed geometry to realize two areas in the specimen that undergo different strain levels along the entire gauge length. In the transition zone, a high plastic deformation was also detected which decreases steeply with increasing the gauge width. Short before failure, high logarithmic strain up to $\varepsilon_{true}$= 0.36 and a high localized deformation region in form of a shear band was found [16].

The influence of different deformation levels in W-temper condition on strengthening behavior of AA6082 is shown in Figure 3 (b). An increase in hardness level in the deformed region compared to the almost undeformed zones is clearly visible. With increasing the global deformation degree, the hardness level increases likewise. The

highest value of 83HV3 of the investigated material is obtained after 18 % deformation.

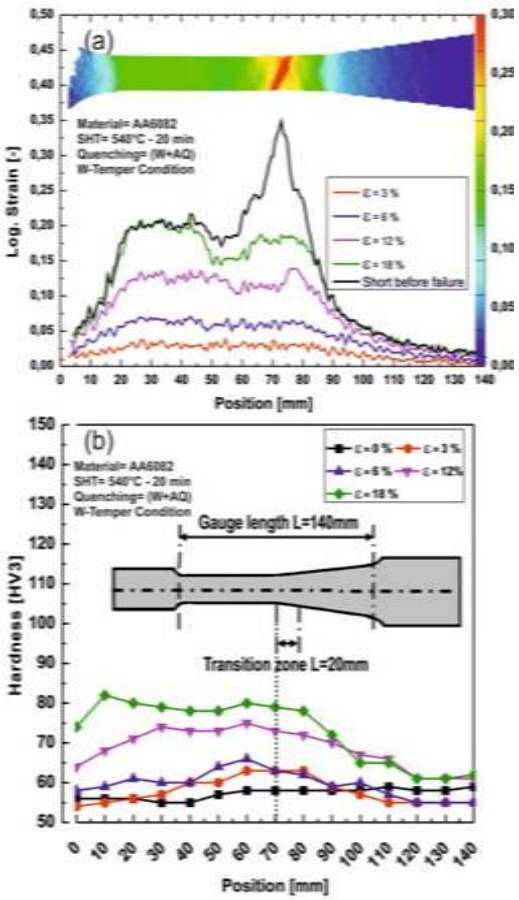


**Figure 3:** Resulting (a) local deformation behavior of AA6082 at different deformation levels and (b) hardness profile along the gauge length of the deformed specimen.

The local deformation behavior of AA7075 during plastic deformation in W-temper condition is represented by the logarithmic strain over the measured length in progression up to failure, Figure 4 (a). Similar to AA6082, the plastic deformation appears mainly in the smallest gauge width and decreases strongly from the beginning of the transition zone to the end (140 mm) of the increasing gauge width. The highest observed logarithmic strain level for AA7075 appears short before failure at a true strain of $\varepsilon_{true}$= 0.28. It can be seen clearly for both materials, plastic deformation appears mainly by mean of high strain localization in the section of reduced width with increasing the global deformation. Initially, as soon as material flow takes place, shear band formation in both alloys appears in shape of band-shaped deformation regions in almost 45° to the load direction. Thus, multiple shear band formation and propagation lead to high ductility under tensional stresses and a large localized plastic strain accomplished with the failure of the specimen.

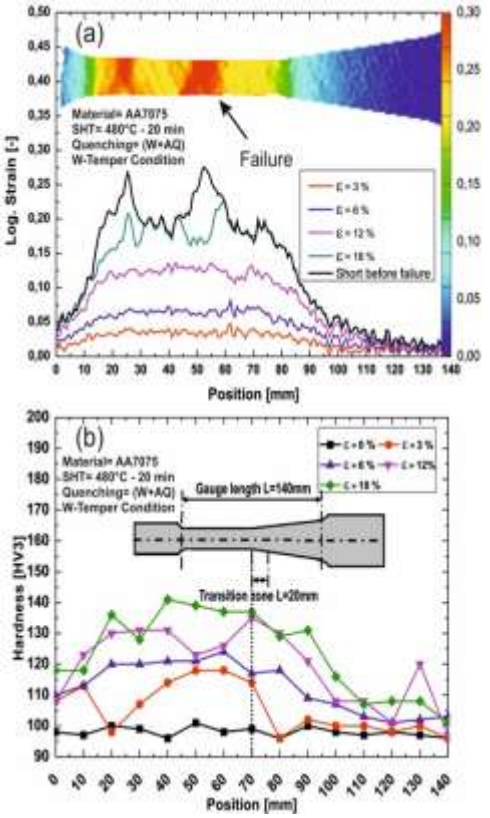


**Figure 4:** Resulting (a) local deformation behavior of AA7075 at different deformation levels and (b) hardness profile along the gauge length of the deformed specimen.

The hardness distribution of AA7075 along the gauge length of the new designed tensile specimen in W-temper is shown in Figure 4 (b). An increase in hardness with increasing the global deformation along the specimen is observed. The highest value is obtained after 18 % global plastic strain in the region with the smaller gauge width. This behavior is linked to the higher dislocation density and strain hardening at higher deformation levels after tensile tests. In the transition zone an increase in the hardness can be seen according to Figure 4 (b), which decreases in direction to the end of the complete gauge length.

### 3.2. Response of age hardening on different deformation levels and gradients

Hardness results of the deformed AA6082 after an artificial aging at 165 °C and 8 hours is shown in Figure 5 (a). The undeformed specimen shows an almost homogenous hardness distribution along the entire gauge length, see black solid line in Figure 5 (a). In contrast, the hardness distribution of all deformed specimens - except for 18 % global strain - indicate higher strength in the highly deformed zone with the smaller gauge width. High hardness values (126HV3) are obtained after 6 and 12 % global deformation. On the contrary, the

lowest value is observed after 18 % global deformation for the same aging condition. Thus, it can be seen from this figure that the strengthening behavior of AA6082 aluminum alloys is improved slightly after 3, 6 and 12 % cold deformation, a higher deformation degree causes lower mechanical properties. However, no dramatic fluctuation of the obtained hardness values along the measurement length was observed.

Figure 5 (b) shows the hardness profile along the gauge length of AA7075 tensile specimen after an aging treatment at 120 °C and 20 hours for different global deformation degrees. The highest hardness level (191HV3) is obtained after 3 % pre-deformed and subsequent aging. At higher deformation levels up to 18 %, the strength of the investigated material decreases slightly, Figure 5 (b). These observations are an evidence for the accelerated precipitation kinetics after cold deformation for both alloys. Consequently, the peak strength can be attained earlier by introducing high dislocation density after plastic deformation.

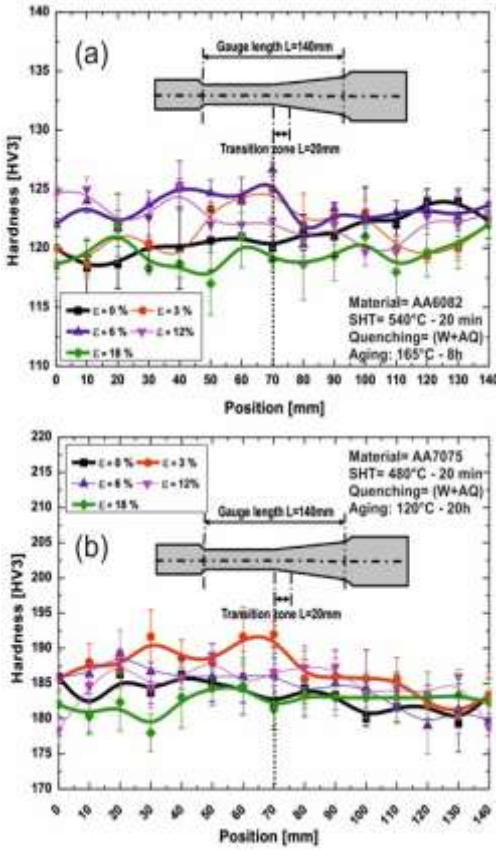


**Figure 5:** Effect of cold deformation on the age hardening of (a) AA6082 and (b) AA7075 after the corresponding aging treatment.

### 3.3. Local strain measurement

The macroscopic deformation behavior for a selection of deformed AA6082 specimen (0, 6 and 18 %) is represented by the logarithmic strain progression up to failure and corresponding local deformation map in tensile direction over the entire gauge length, Figure 6 (a-c). As it can be seen for the undeformed stage, plastic deformation appears mainly homogenously up to the necking point. After necking, high local deformation up to $\varepsilon_{true}$= 0.32 and a distinct reduction in area was found. A similar strain map is observed for the 6 % deformed specimen. The determined deformation map indicates a homogeneous strain distribution along the entire gauge length up to the necking point. Interestingly, the measured logarithmic strain shortly before failure is more localized compared to the undeformed specimen. In contrast to those conditions, plastic deformation of the 18 % deformed specimen appears mainly in the region of reduced width and the transition zone (10 – 86 mm), which underwent a high plastic deformation in the pre-straining process of WP 1, Figure 3 (a). Taking this phenomenon into the account, it is clearly shown that the strength in this region is reduced and hence plastic deformation takes place preferrably in the softer region of the tensile specimen. It should be further noticed that with increasing the pre-deformation level lower elongation to failure is obtained.

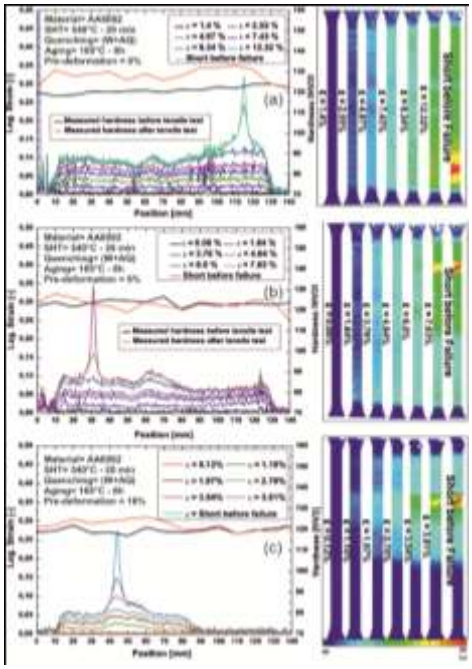


**Figure 6:** Local deformation behavior of (a) undeformed sample, (b) after 6 % and (c) 18 % pre-deformation with the corresponding local strain map of AA6082 after aging treatment.

Figure 7 (a-c) shows the local deformation map and local strain progression short before failure of the selected deformed AA7075 specimen (0, 6 and 18 %) after aging at 120 °C for 20 hours. Up to the point of necking, a uniform strain distribution was observed for the undeformed and 6 % pre-deformed specimen. After the neck has formed, plastic deformation concentrates mainly in the smallest gauge width in case of the deformed specimen. However, higher logarithmic strain $\varepsilon_{true}$= 0.27 was observed for the undeformed specimen, which corresponds to higher formability. At higher pre-deformation levels, deformation heterogeneity is observed that takes place in different regions of the tensile specimen as shown in the strain map, Figure 7 (c). With continuous increasing the tensile stress and deformation level up to failure, the sample deforms predominantly in this section with the smallest gauge width. It should be further noted that no propagating deformation band after aging was observed for both investigated alloys.

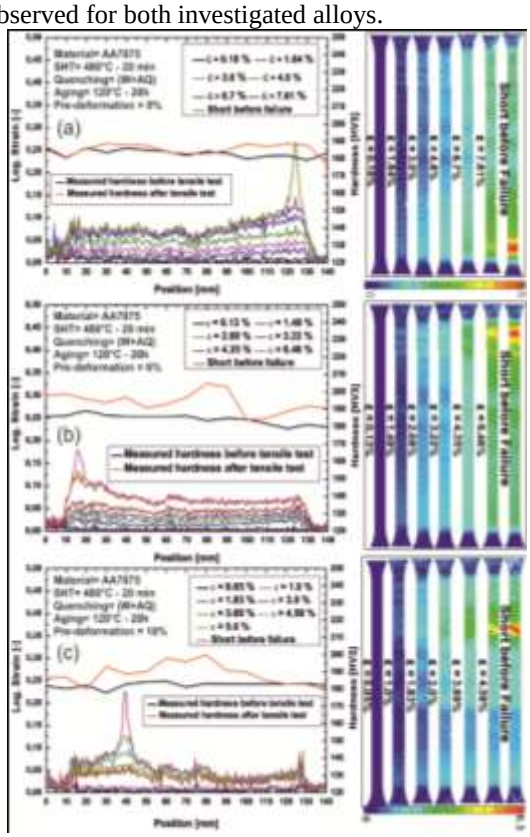


**Figure 7:** Local deformation behavior of (a) undeformed sample, (b) after 6 % and (c) 18 % pre-deformation with the corresponding local strain map of AA7075 after aging treatment.

## IV. CONCLUSION

The present study provides insight into the influence of different cold deformation gradients on precipitation kinetics and the resulting mechanical properties of two different aluminum alloys AA6082 and AA7075. Summing up, following major conclusions are drawn:

Both aluminum alloys show a high formability and lower material strength during W-Temper forming up to failure. This behavior is due to the as-quenched condition of the investigated materials and the fully dissolved alloying elements inside the aluminum matrix. The underlying reason is, that the dislocation movement is not impeded by precipitates and other second phases.

The level of strain hardening in W-temper forming depends on the local strain distribution. With increasing global strain the maximum hardness increases, but also the hardness gradient in the tapered section according to the strain gradient. This is a direct consequence of the local dislocation density, which represents the amount of obstacles for dislocation movement.

The response of age hardening on W-temper deformation at room temperature shows in general only a slight effect. However, depending on the global strain level and on the alloy composition a distinct hardness distribution was observed along the entire specimen reflecting the different levels of deformation. This particular behavior can be explained by the assumption that dislocation accumulation accelerates the aging processes resulting in a distribution of varying precipitates and second phase morphologies.

Tensile tests after aging coupled with DIC of standard geometry reveal for the undeformed and 6 % pre-deformed samples a uniform strain distribution up to the point of necking. At higher deformation level, plastic deformation appears mainly in the region with higher cold deformation degree. This phenomenon can be attributed to a coagulated state of the precipitates leading to softening.

## ACKNOWLEDGEMENTS

The author would like to thank the Hessen State Ministry for Higher Education, Research and the Arts – Initiative for the Development of Scientific and Economic Excellence (LOEWE) for the financial support of the special research project "ALLEGRO".

## REFERENCES

[1]. E.A. Starke, J.T. Staleyt, Application of Modern Aluminum Alloys to Aircraft, Prog. Aerospace Sci. 32 (1996) 131–172.

[2]. E. Samuel, Application of the Hot Stamping Process to Aluminum Alloy Structural Components, Springer, Cham, 2018: pp. 301–306. doi:10.1007/978-3-319-72284-9_41.

[3]. M. Merklein, M. Lechner, A. Kuppert, Enhancement of formability of aluminum alloys in multi-stage forming operations by a local intermediate heat treatment, Production Engineering. 6 (2012) 541–549.

[4]. E.A. Starke, Y. Khalfalla, K.Y. Benyounis, Aluminum Alloys: Thermomechanical Processing, Reference Module in Materials Science and Materials Engineering. (2016).
[5]. E. Scharifi, R. Knoth, U. Weidig, Thermo-mechanical forming procedure of high strength Aluminum sheet with improved mechanical properties and process efficiency, Procedia Manufacturing. 29 (2019) 481–489.
[6]. Y. Liu, L. Wang, B. Zhu, Y. Wang, Y. Zhang, Identification of two aluminum alloys and springback behaviors in cold bending, Procedia Manufacturing. 15 (2018) 701–708.
[7]. A. Wang, K. Zhong, O. El Fakir, J. Liu, C. Sun, L.L. Wang, J. Lin, T.A. Dean, Springback analysis of AA5754 after hot stamping: experiments and FE modelling, International Journal of Advanced Manufacturing Technology. (2016) 1–14..
[8]. N. Bay, Cold forming of aluminium—state of the art, Journal of Materials Processing Technology. 71 (1997) 76–90. doi:10.1016/S0924-0136(97)00152-0.
[9]. E.S. de Argandoña, L. Galdos, R. Ortubay, J. Mendiguren, X. Agirretxe, Room Temperature Forming of AA7075 Aluminum Alloys: W-Temper Process, Key Engineering Materials. 651–653 (2015)199–204.
[10]. O. Jensrud, K. Pedersen, Cold forging of high strength aluminum alloys and the development of new thermomechanical processing, Journal of Materials Processing Technology. 80–81 (1998) 156–160.
[11]. Y. Lu, J. Wang, X. Li, W. Li, R. Li, D. Zhou, Effects of pre-deformation on the microstructures and corrosion behavior of 2219 aluminum alloys, Materials Science and Engineering: A. 723 (2018) 204–211.
[12]. L. AN, Y. CAI, W. LIU, S. YUAN, S. ZHU, F. MENG, Effect of pre-deformation on microstructure and mechanical properties of 2219 aluminum alloy sheet by thermomechanical treatment, Transactions of Nonferrous Metals Society of China. 22 (2012) s370–s375.
[13]. M. Gazizov, R. Kaibyshev, Effect of pre-straining on the aging behavior and mechanical properties of an Al-Cu-Mg-Ag alloy, Materials Science and Engineering A. 625 (2015) 119–130.
[14]. M. Fujda, M. Matvija, P. Horňak, Effect of Pre-Straining and Natural Aging on the Hardening Response during Artificial Aging of EN AW 6082 and Lead Free EN AW 6023 Aluminium Alloys, Materials Science Forum. 952 (2019) 82–91.
[15]. E. Scharifi, D. Kuhnhenn, A. Ademaj, U. Weidig, An Experimental Investigation of Hot Forming Effects on Mechanical Properties of High-Strength Aluminum Alloys AA6082 and AA7075, K. Steinhoff, M. Oldenburg, B. Prakash, (Edtrs.), Proc. 6th Int. Conf. Hot Sheet Met. Form. High-Performance Steel, Warrendale AIST. (2017) 683–690.
[16]. H. Aboulfadl, J. Deges, P. Choi, D. Raabe, Dynamic strain aging studied at the atomic scale, Acta Materialia. 86 (2015) 34–42.

Emad Scharifi" Influence of plastic deformation gradients at room temperature on precipitation kinetics and mechanical properties of high-strength aluminum alloys" International Journal of Engineering Research and Applications (IJERA), Vol. 09, No.06, 2019, pp. 42-48